Sensing unrest in New Zealand's largest city: detailed mapping of seismicity in Auckland

Prepared by: Calum John Chamberlain[1*], Jenni Hopkins[1], John Townend[1], Kasper Van Wijk[2] and Nathanial Lindsey[3]

1: Victoria University of Wellington

2: University of Auckland

3: FiberSense

* calum.chamberlain@vuw.ac.nz

26 June 2025

With funding support from

Natural Hazards Commission
Toka Tū Ake

Acknowledgements

This project is supported by a Natural Hazards Commission Toka Tū Ake biennial research fund. Support is provided by Victoria University of Wellington (Chamberlain, Hopkins and Townend), University of Auckland (van Wijk) and FiberSense (Lindsey). This project is aligned with and has informed by Natural Hazards Commission Toka Tū Ake University Research Programme in Earthquake Seismology and Tectonic Geodesy. Chamberlain is supported by a Rutherford Discovery Fellowship from the Royal Society Te Apārangi. We acknowledge the New Zealand GeoNet programme and its sponsors NHC Toka Tū Ake, GNS Science, LINZ, NEMA and MBIE for providing data used in this study.

Executive Summary

The Auckland Volcanic Field presents a significant hazard to New Zealand's largest city. It is expected that volcanic unrest would be preceded by elevated earthquake rates. Present knowledge of the background state of seismicity is limited by the nationwide focus of the GeoNet earthquake cataloguing workflow, and variations in cataloguing methods over the last two decades. Alongside this, high levels of seismic noise due to human activity make it difficult to detect small earthquakes using conventional seismic sensors.

We demonstrate that by using a targeted approach to cataloguing earthquakes within the Auckland Volcanic Field we can robustly detect and locate more than 5 times as many earthquakes as are in the GeoNet catalogue. From this we show that earthquake sequences occur in the Auckland Volcanic Field without volcanic unrest. To enable robust analysis of future earthquake sequences in the Auckland Volcanic Field we recommend adopting a similar targeted approach to earthquake cataloguing, and suggest that routine focal mechanism or moment tensor determination should be applied to all earthquakes within the Auckland Volcanic Field.

To enable enhanced earthquake monitoring in urban settings we test earthquake detection applied to Distributed Acoustic Sensing data recorded on telecommunications fibre-optic cables. Due to low earthquake rates in Auckland, we test these using a fibre in Wellington. We find that although this new data can provide enhanced earthquake detection in urban settings, it is likely to be best used in combination with conventional instruments to reduce false detections.

Abstract

The Auckland Volcanic Field presents a significant hazard to New Zealand's largest city. It is expected that volcanic unrest would be preceded by elevated earthquake rates. Present knowledge of the background state of seismicity is limited by the nationwide focus of the GeoNet earthquake cataloguing workflow, and variations in cataloguing methods through time. Alongside this, high levels of seismic noise due to human activity make detecting small earthquakes using conventional seismic sensors difficult. We detect and locate more than 5 times as many earthquakes as are in the GeoNet catalogue using a machine-learning enhanced, semi-automated workflow. We observe nine sequences of more than five earthquakes in the 11-year study period. We also test earthquake detection applied to Distributed Acoustic Sensing data recorded on telecommunications fibre-optic cables to understand if such data can be used to enhance earthquake detection in urban settings. Due to low earthquake rates in Auckland, we test these using a fibre in Wellington. We find that although this new data can provide enhanced earthquake detection in urban settings, it is likely to be best used in combination with conventional instruments to reduce false detections.

Keywords

Earthquake, Volcanoes, Machine Learning, Distributed Acoustic Sensing, Quantifying hazards and risk

Introduction

The Auckland Volcanic Field (AVF) poses a substantial hazard to New Zealand's largest city (Hopkins et al., 2021) . Volcanic unrest in the AVF is expected to be preceded by elevated rates of seismicity, which may provide warning of an impending eruption (Sherburn et al., 2007). The low but non-zero rates of seismicity within the AVF (Figure 1) coupled with limitations on earthquake detection imposed by methodological choices, and variations in those choices through time, mean that the background state of the AVF is hard to characterise. Without a robust understanding of the background state of seismicity, and hence what variations could be expected without unrest, it is difficult to provide useful quantification of any future unrest.

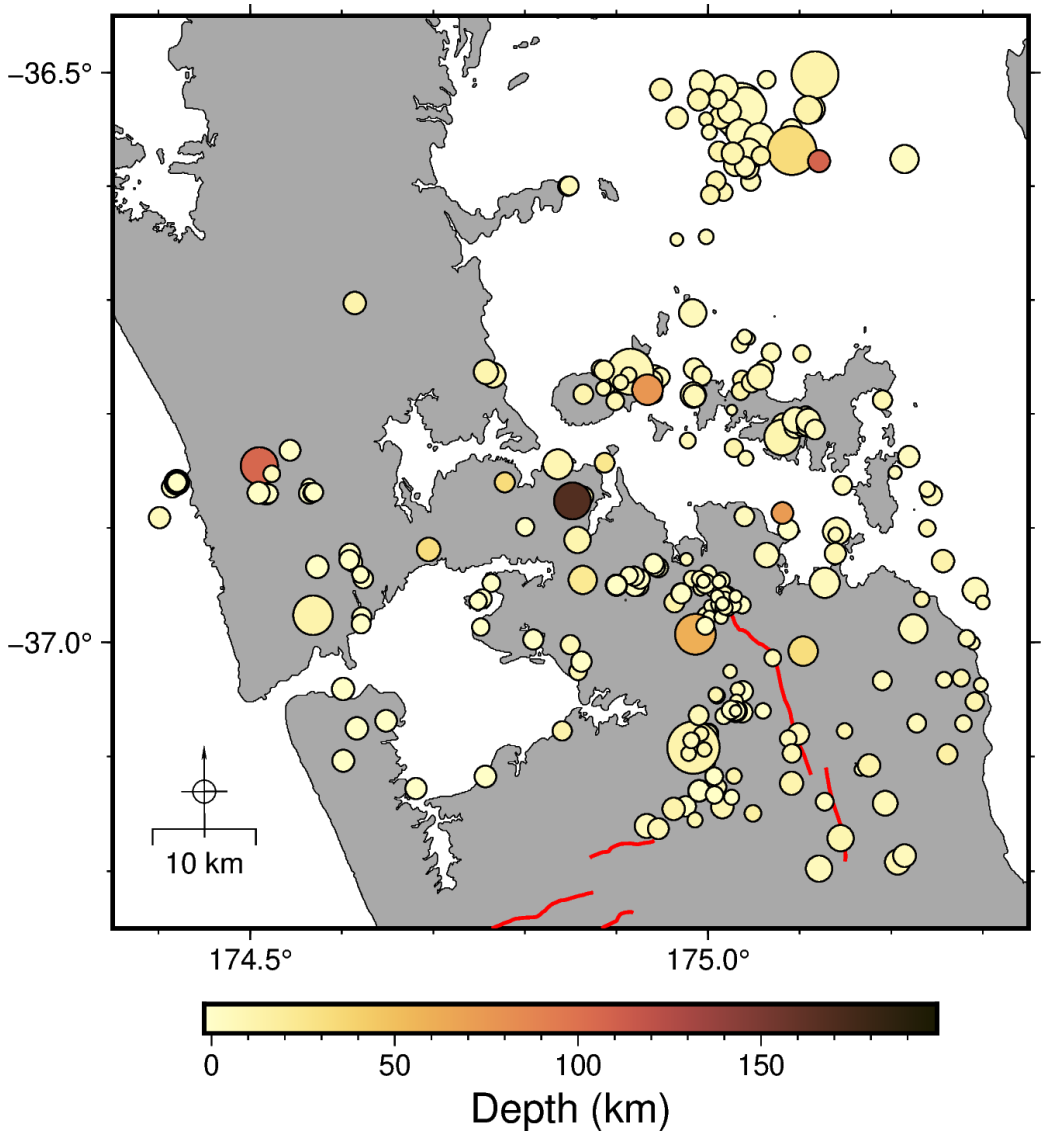

Figure 1: GeoNet catalogue 1987-2024 plotted as coloured circles, sized by magnitude. Red lines delineate active fault traces from the NZ Active Fault Database (Langridge et al., 2016).

In this project we applied state-of-the-art methods to seismic data from the AVF over a 11-year period to generate the first long-duration, self-consistent catalogue of seismicity within the AVF. Alongside this analysis, we tested and developed earthquake detection methods on a relatively new type of seismic data using Distributed Acoustic Sensing (DAS) measurements recorded on telecommunications cables. Due to limited seismicity within the AVF during our project, we developed these methods using data from fibres in Wellington using data collected by commercial partner: FiberSense.

Seismicity of the Auckland Volcanic Field

Within New Zealand, the Auckland region is notable for low levels of seismicity, with only 383 seismic events (184 labelled as earthquakes; the remainder are most commonly labelled as explosions) catalogued by New Zealand's national earthquake monitoring agency, GeoNet between 1835 and 2024. Earthquake detection in Auckland is hampered by high levels of anthropogenic noise (Van Wijk et al., 2021), although the Auckland Volcano Seismic Network operated by GeoNet is dense, and has several (7, Figure 2) borehole stations in an attempt to reduce the impact of anthropogenic noise on earthquake detection.

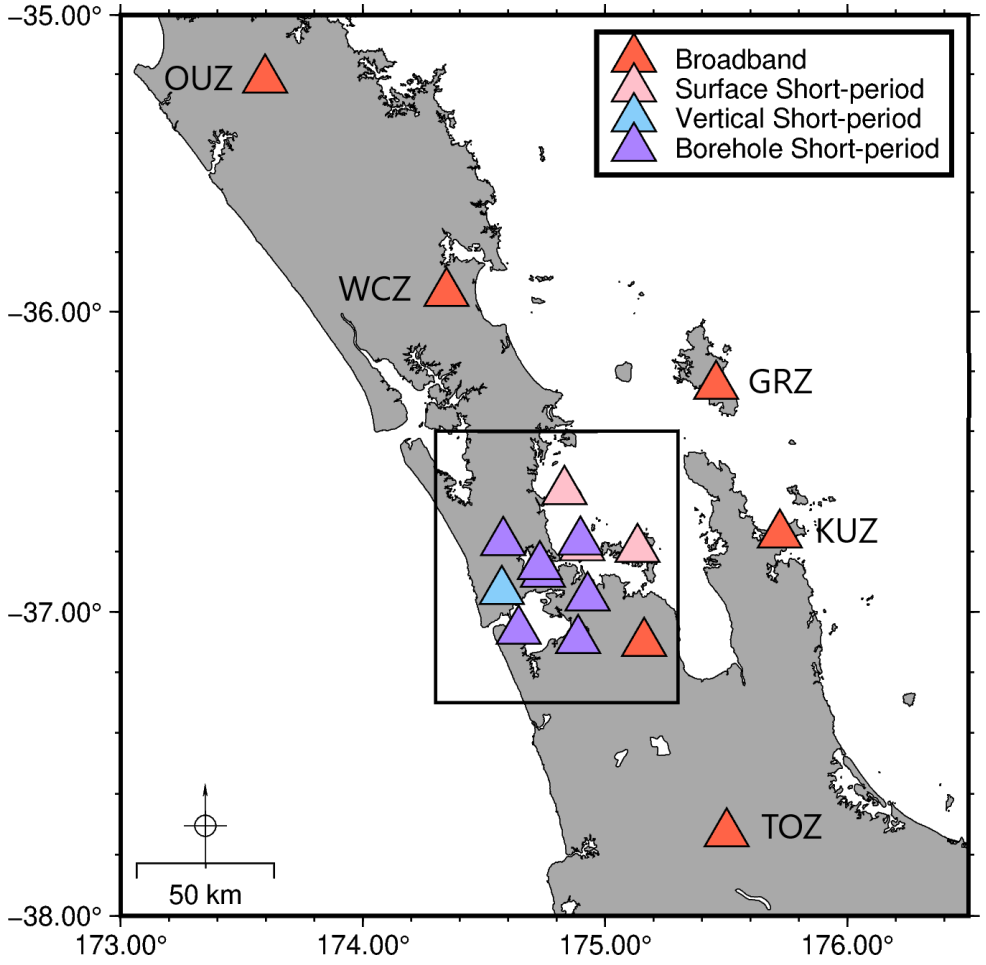

Figure 2: GeoNet network around the AVF. Black box shows region plotted in Figure 1 which is our main study area.

The current (at the time of writing) GeoNet earthquake detection settings require detection on at least ten stations. Within the AVF there are 12 seismic stations integrated into the national monitoring network (Figure 2), however only 11 have operated contemporaneously. As such, high noise levels, or low signal amplitudes, at only two stations will result in non-detection of local seismicity. Alongside the use of relatively high detection criteria, GeoNet, presently uses the IASP91 global 1D seismic velocity model (Kennett & Engdahl, 1991) for earthquake location, which not only has significantly different crustal velocities to those imaged beneath the AVF, but also fails to capture the significant 3D variability in seismic velocity beneath the AVF (Ensing et al., 2017, 2022), likely resulting in poor quality locations.

Earthquake monitoring practices, and station availability throughout New Zealand, including the AVF, have changed through time (Figure 3). While little can be done to cope with changes to station availability, the changes in monitoring tools and parameters lead to variability in the earthquake catalogue that can be overcome by re-analysis. These changes in monitoring methods have not been well documented, making it hard to untangle the influence of physical changes to the monitoring changes and monitoring practice changes.

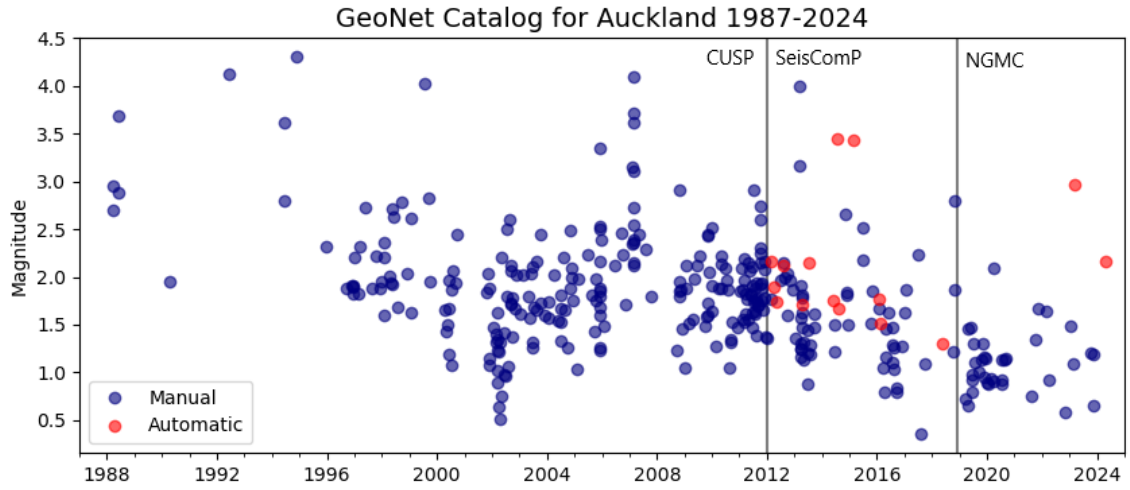

Figure 3: Magnitude and time for earthquakes in the GeoNet catalogue since the CUSP analysis technique was introduced. Major documented changes to observational practice are marked by vertical lines. The change in 2012 represented a software change from CUSP to SeisComP. The change in 2016 was the introduction of the National Geohazard Monitoring Centre (NGMC). Note that pre-SeisComP all earthquakes had manual review. Following the change to SeisComP additional automatic processing was introduced. Following the change to NGMC processing, most events were again manually reviewed. The general reduction in lowest magnitude is partly related to improvements to the monitoring network.

The variability in the GeoNet catalogue makes it impossible to robustly quantify and characterise the background state of seismicity within the AVF: a key pre-requisite to accurately determining if any future seismicity is part of the background state, or unexpected and possibly related to volcanic unrest. In this work we construct a new, self-consistent catalogue of earthquakes within the AVF using advanced machine-learning earthquake detection tools, alongside manual quality checking.

Distributed Acoustic Sensing for earthquake analysis

DAS applied to fibre-optic cables is providing new ways to sample the seismic wavefield at high spatial resolution (Lindsey & Martin, 2021; Lindsey et al., 2017). In particular, DAS methods applied to telecommunications fibres provide a way of sensing the seismic wavefield in urban environments, making them potentially well suited to the study of seismicity in the AVF (Nayak et al., 2021).

DAS uses an “interrogator” to probe fibre-optic cables using laser pulses (Lindsey & Martin, 2021). The interrogator measures the optical phase of backscattered light from the length of the cable. Changes in optical phase can be related to strain changes along the length of the fibre and can be used to effectively provide recordings of the seismic wavefield every few metres along the fibre path. Previous work has shown that DAS is sensitive to seismic phases, although fibres are only sensitive to motion parallel to the fibre, in contrast to three-component seismometers.

Recent work has shown that DAS measurements can be used to record (Lindsey et al., 2020), detect (e.g. Li & Zhan, 2018), locate (e.g. van den Ende & Ampuero, 2021) and resolve focal mechanisms (Li et al., 2023) of earthquakes, amongst other applications. In our work we aim to assess the potential for DAS to provide enhanced seismic monitoring in urban environments such as the AVF. To test this requires an urban DAS deployment and near-fibre seismicity detected by other, well-tested methods to compare to.

Objectives

Our project was developed to address three main research objectives:

1) Construct a dense, continuous catalogue of AVF earthquakes since 2012 using machine-learning detection methods to measure background seismicity rates in the AVF.
2) Accurately constrain the locations and focal mechanisms of earthquakes detected in objective 1 to characterise active faulting beneath the AVF.
3) Develop new tools for enhanced detection, location and characterisation of seismic and volcanic hazards in urban environments using conventional and DAS datasets.

Our project successfully met objective one and partially met objective two: additional manual analysis to robustly quality-control the earthquake locations meant that there was not enough time within the project-supported MSc student's study to compute focal mechanisms. Within objective three, we modified and enhanced earthquake detection methods developed by the research team to DAS data and demonstrated their efficacy and limitations for DAS data in urban settings during high-rate sequences similar to those expected during volcanic unrest. This knowledge has also helped inform aligned projects on earthquake analysis of DAS data also supported by NHC.

In this project we make use of two distinct datasets: 1) the long-term GeoNet dataset of seismic waveforms recorded around the AVF between 2011 and 2022; 2) continuous, downsampled DAS data recorded on two telecommunications fibres in Wellington around known earthquakes. Dataset 1 was used for objectives one and two, while Dataset 2 was used for objective three. We note that we were unable to use fibre data from Auckland to develop earthquake detection methods, mostly due to the low rate of seismicity in Auckland which resulted in a poor testcase for earthquake analysis. Nevertheless, our findings from Dataset 2 should be transportable to other fibres, and the codes and techniques developed through this project are designed to be agnostic to data source. For clarity, the remainder of this report is separated into these two sub-projects.

Analysis of AVF seismicity

Methodology

To enable efficient analysis of the long-duration seismic dataset required to develop such a long-duration catalogue we developed a semi-automated workflow tailored to the AVF network. We first retrieved all waveforms for weak-motion seismic stations within the bounds 174.5–175.25°longitude and -37.25—36.4°latitude. These twelve stations form the backbone of the Auckland Volcano Seismic Network (AVSN). We supplemented these data with five additional GeoNet broadband sites within 200 km of the AVF (Figure 2). For this composite network we downloaded data between 01/01/2011–01/01/2022 from the GeoNet Amazon Web Services public S3 bucket. Of this network, six stations have broadband instruments, and the remaining eleven have short-period sensors. All stations apart from WTAZ have three-component sensors: WTAZ has a single-component vertical seismometer. Of the 11 short-period sites, seven are installed in boreholes to reduce the impact of anthropogenic noise. Of this network, a maximum of 16 sites were operational at any time, with MTAZ replaced by MBAZ in 2012.

To enable robust, self-consistent analysis of the long-duration dataset we chose to use the EQTransformer (Mousavi et al., 2020) machine-learning model to detect and pick earthquakes. We used the implementation of EQTransformer in seisbench (Woollam et al., 2022), and the weights trained on the STEAD database (Mousavi et al., 2019). This model has been shown to have good accuracy in other regions of New Zealand (Pita-Sllim et al., 2023) with similar data, when using overlapping windows with large overlaps. We note that EQTransformer is designed to use three-component data: for the single-component station used here (WTAZ), we copy the vertical component data into two additional channels as suggested by Mousavi et al. (2020).

We tested the parameterisation of EQTransformer by comparing the performance of EQTransformer to the known events in the GeoNet catalog, and compared to both GeoNet picks, and our own manual picks of those GeoNet events. We chose to use an overlap length of 55 s (for the 60 s windows processed by EQTransformer) as suggested by Pita-Sllim et al. (2023). Such large overlaps can result in duplicate detections and picks. To ameliorate this we combined output probability time-series by taking the average of overlapping sections as implemented in seisbench. We found that taking the maximum of overlapping windows resulted in more duplicate picks than taking the average, but with similar performance (pick-time differences were on average less than 0.04 s for both P (Figure 4) and S picks, compared to either our manual picks or the GeoNet picks). We found that a threshold of 0.01 gave low-levels of false detections when averaging probability time-series windows and used this threshold for both P and S picks.

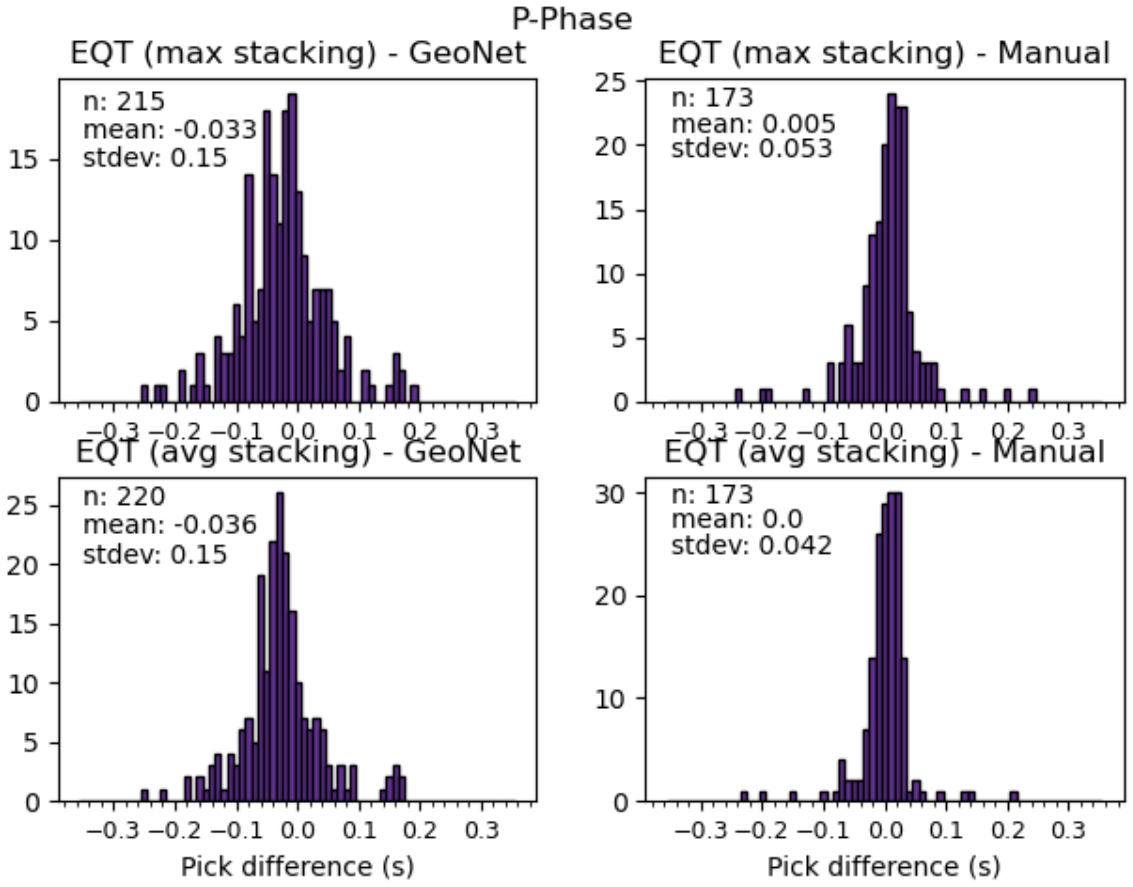

Figure 4: Pick-time differences for P-phase observations comparing automatic EQT (EQTransformer) picks to GeoNet (left) and our manual (right) picks. Upper row shows picks made using "max" stacking of overlapping probability time-series. Lower panel shows "avg" (average) stacking of probability time-series.

To associate picks from discrete stations into picks from individual events we tested two recent phase association tools: GaMMA (Zhu et al., 2022) and PyOcto (Münchmeyer, 2024). In testing we used the same 1D velocity model for both associators and included pick amplitudes in GaMMA as this can help separate overlapping events (Münchmeyer, 2024). For both GaMMA and PyOcto we set a minimum of five associated picks to define an event, and for PyOcto we required at least 2 picks of both P and S phases to define an event, and at least two stations with both P and S picks. We found from testing on picks from three randomly selected months that PyOcto resulted in fewer false associations, or associations of real regional or teleseismic events, but with incorrect locations within the study region. We trialled various parameter settings for PyOcto and found that requiring at least two stations with both P and S picks helped to reduce the number of incorrectly associated/located regional or teleseismic events.

We located our associated events using NonLinLoc (Lomax et al., 2000), which solves the non-linear earthquake location problem using grid-search methods over a grid of possible locations. We used the NZ3D velocity model of (Eberhart-Phillips et al., 2010), version 2.2 for location. Due to relatively poor ray-path coverage in the AVF, this model is coarsely

sampled and likely has moderate uncertainties. We therefore chose to set a model-derived travel-time uncertainty of 5% of the travel-time. We only located events that had PyOcto computed locations within the region of interest, defined as between 174.0–175.5° longitude and -37.5- -36.0° latitude.

To remove incorrectly associated PyOcto-located events we applied a depth and pick-dependent quality control. We found that generally deeper events had a higher incidence rate of incorrect locations and we therefore chose to require more picks for events with deeper PyOcto locations. We retained all events shallower than 30 km. For events with initial depths between 30–50 km we required at least 3 stations with both P and S picks. For earthquakes with initial depths greater than 50 km we required at least ten picks, with at least three stations with both P and S picks.

Our initial testing showed a non-zero false detection rate, and that both earthquakes and quarry blasts were picked by EQTransformer. To remove false detections and to separate quarry blasts and earthquakes we manually reviewed all located events by visual inspection of waveforms overlain with pick times. We generally identify quarry blasts as having anomalously high surface wave energy, and/or lacking S arrivals. We also note that quarry blasts are more common during weekdays during business hours and therefore take this into consideration when assessing event type.

Finally, we compute magnitudes for all events. We make automatic amplitude measurements using EQcorrscan (Chamberlain et al., 2018) and derive Wood-Anderson equivalent amplitudes. We then use these amplitudes in the recently updated NZ-wide local magnitude scale, MLNZ20 (Christophersen et al., 2022). We note that all stations used here have station correction terms computed for them by Christophersen et al. (2022), hence we do no re-evaluation for our specific network.

Results and discussion

We made c. 1.17 million picks (735,000 P and 434,000 S) using EQTransformer. These picks were associated in 19,800 events using PyOcto. Of these events only 18% (3,564) met our initial quality control criteria for location. Most events that did not meet our location quality criteria were located outside the region of interest. Of these events, 7 were unable to be located with NonLinLoc due to having picks inconsistent with physical hypocentres. After manual quality control we determined that 42% (1,498) events were detections not of interest (out of the region of interest, but falsely associated with hypocentres within our region of interest), 40% (1,428) were quarry blasts or similar anthropogenic sources, and 17% (611) were true earthquakes. We were not able to classify confidently the remaining 20 events. Our final locations are shown in Figure 5. Within our region of interest (bounded by 36.5- -37.2 S latitude and 174.4-175.3 E longitude) there are 368 earthquakes.

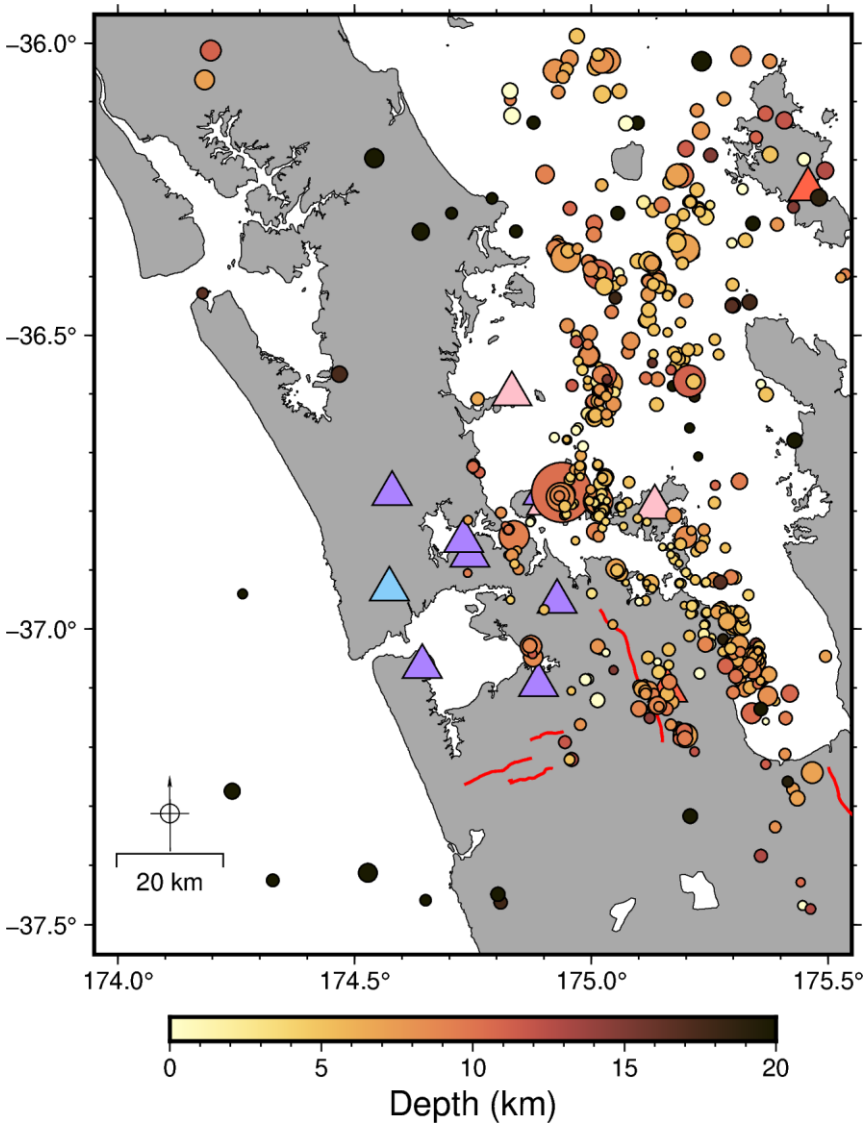

Figure 5: Earthquake locations in the AVF. Note events deeper than 20km are coloured black.

Our catalogue is dominated by earthquakes to the east of our network, resulting in relatively high location uncertainties. The average 68% depth uncertainty for the catalogue as a whole is 3.8 km, and the average 68% horizontal uncertainty is 3.7 km. These uncertainties generally decrease within the network footprint. We note that there is a concentration of locations around 5 km depth which is likely a location artefact. Eleven earthquakes have negative depths, however the depth uncertainties for these earthquakes are larger than their elevations.

We resolve magnitudes ranging from -0.5 to 3.9. Over the same time-period for the same region GeoNet report 65 events between 0.4 and 3.9 magnitude. Note that the magnitudes reported in the GeoNet catalogue are not consistent throughout the duration of the catalogue, making any comparison of magnitudes difficult. Our catalogue has a magnitude of completeness of 0.6 as calculated by both the maximum curvature method and the goodness-of-fit method. The best fit Gutenberg-Richter distribution for our catalogue has a relatively low b-value of 0.8. Due to the low numbers of earthquakes in our catalogue, we are unable to robustly evaluate changes in completeness or b-value through time, however given the station continuity throughout the study period we expect changes in completeness to be minimal.

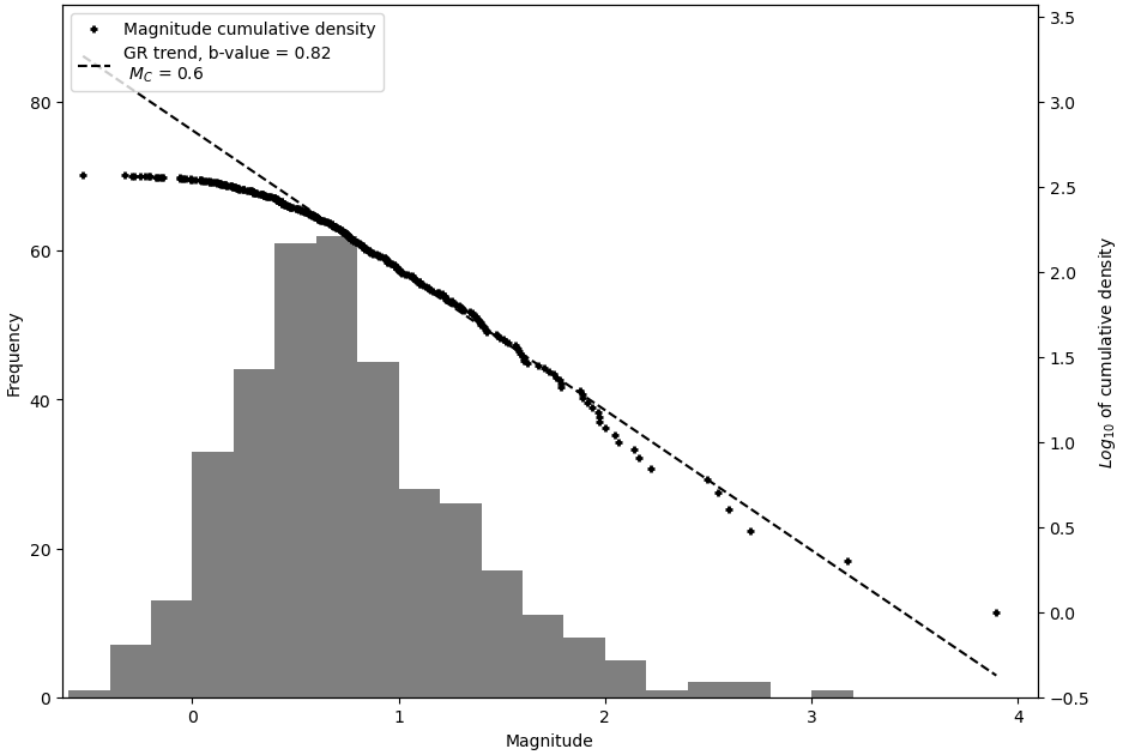

Figure 6: Magnitude-frequency distribution for our AVF earthquake catalogue within the region 36.5--37.2 S latitude and 174.4—175.3 E longitude (N=368).

Of the 368 earthquakes in the AVF study region, the background rate across the whole dataset is 1 earthquake every 11 days. Inter-event times ranged from 14 seconds to 72 days, with a median inter-event time of 3.8 days. For events above the magnitude of completeness of 0.6, inter-event times range from 16 seconds to 160 days with a median of 7.8 days.

Clusters of earthquakes exist in the catalogue (Figure 7) where rates spike as high as 12 earthquakes per day (using a 10-event moving window). Three sequences with more than ten earthquakes per day occurred in the dataset in 2011, 2013 and 2016. The sequence in 2011 began on 30/09/2011 and lasted 2.5 days containing 12 earthquakes between M 0.7 and M 2.2. Half the earthquakes in this sequence were catalogued by GeoNet. The second sequence in 2013 started on 17/03/2013 and lasted 35 days containing 29 earthquakes between M 0.1 and M 3.9. Of this sequence, 13 earthquakes are in the GeoNet catalogue. The final major sequence of 15 earthquakes between M 0.2 and M 1.4 started 21/11/2016 and lasted two days. Only one of these earthquakes (the largest) is in the GeoNet catalogue. Six further sequences of five to nine events also occurred in our analysis period.

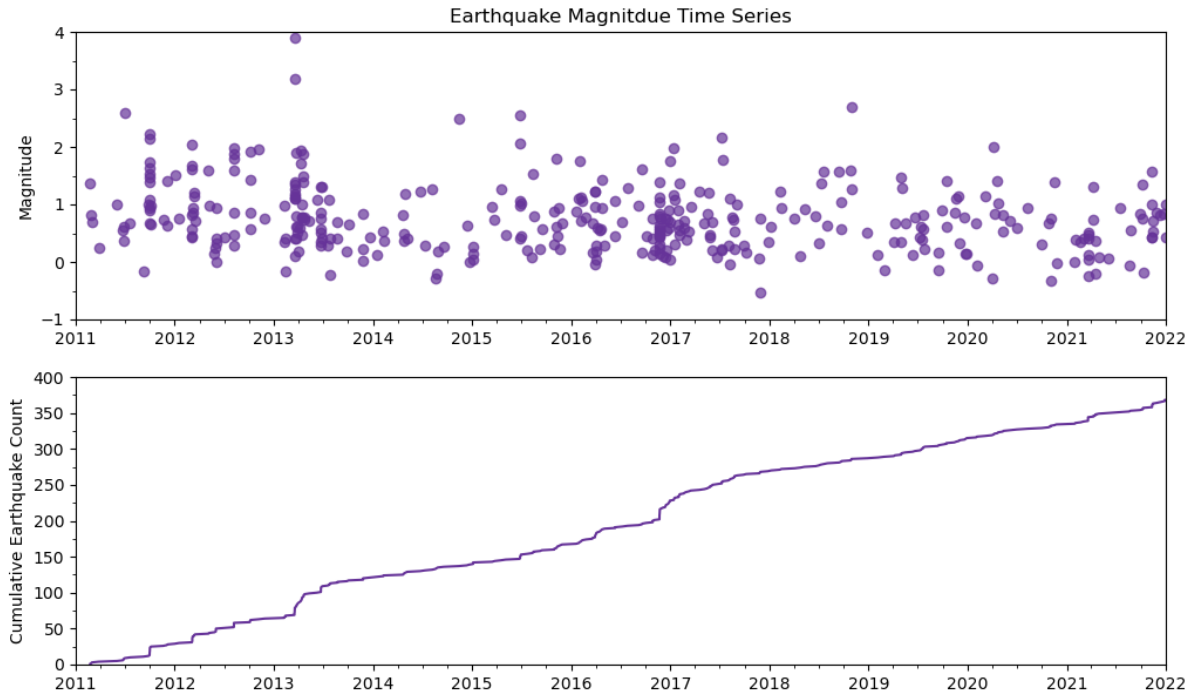

Figure 7: AVF earthquake occurrence times. Top panel: magnitude against time. Bottom panel: Cumulative earthquake numbers against time. Note steps in cumulative time-series corresponding to high-rate sequences.

Conclusions and Recommendations:

Our analysis demonstrates that there are significantly more earthquakes within the AVF than catalogued by GeoNet. Nevertheless, the background rate of earthquakes is low (1 earthquake every 11 days on average), but this rate is variable. Much of this variability is lost in the GeoNet catalogue due to the relatively high magnitude of completeness despite the dense station spacing. While earthquake clusters do occur in our catalogue, they are relatively rare compared to other volcanic regions in New Zealand (only 9 sequences of more than five events in the 11-year study period). The earthquake sequences we document also have variable durations, highlighting that the occurrence of earthquake clusters alone should not be enough to imply volcanic unrest.

From this work we recommend that such a focused approach to earthquake cataloguing in the AVF is necessary to robustly characterise changes in earthquake occurrence if this is to be used to volcanic monitoring. We also suggest that routine focal mechanism of moment tensor analysis in the AVF would be necessary to provide a better understanding of the source of any future earthquake sequences here.

Earthquake detection with DAS

Methodology

Within this project we tested the application of two well-established methods to new DAS data in Wellington. DAS data provide dense sampling of the seismic wavefield, making these data well-suited to methods developed for dense seismic arrays. We trialled FK (Frequency-Wavenumber) filtering to remove noise not associated with earthquake arrivals, and matched-filter earthquake detection to provide enhanced earthquake detection. Matched-filter methods are well-known to de able to detect earthquakes with signal amplitudes at or below the noise level of the data. Because DAS data are inherently noisy, but have good spatial coherency, network wide matched-filters appear to be a good choice for earthquake detection using DAS in particular circumstances (Li & Zhan, 2018).

With conventional seismological data, where seismometers are often separated by kilometres to tens of kilometres, the delay in the arrival of seismic waves between different seismometers is a strong discriminator of source location within matched-filter detection algorithms (Chamberlain & Townend, 2018). We wanted to test whether the same would be true for such high spatial density datasets as DAS to determine whether matched-filters applied solely to DAS data could effectively discriminate between different earthquake sources.

We focused our analysis on data recorded around the April 2023 M5.9 Porangahau earthquake and its aftershocks (Figure 8). This earthquake sequence provided a good test dataset to compare DAS detections against detections made by GeoNet. We also used this dataset to trial the impact of FK filtering of earthquake detectability. We used the Vodafone operated fibre surrounding the Wellington harbour. Details of the fibre path remain commercially sensitive and are not provided here. The first ~35km of the fibre path are on-land, before going offshore across the harbour. Once back onshore, several sections of the cable are strung above ground resulting in poor recovery of seismic energy (Figure 9).

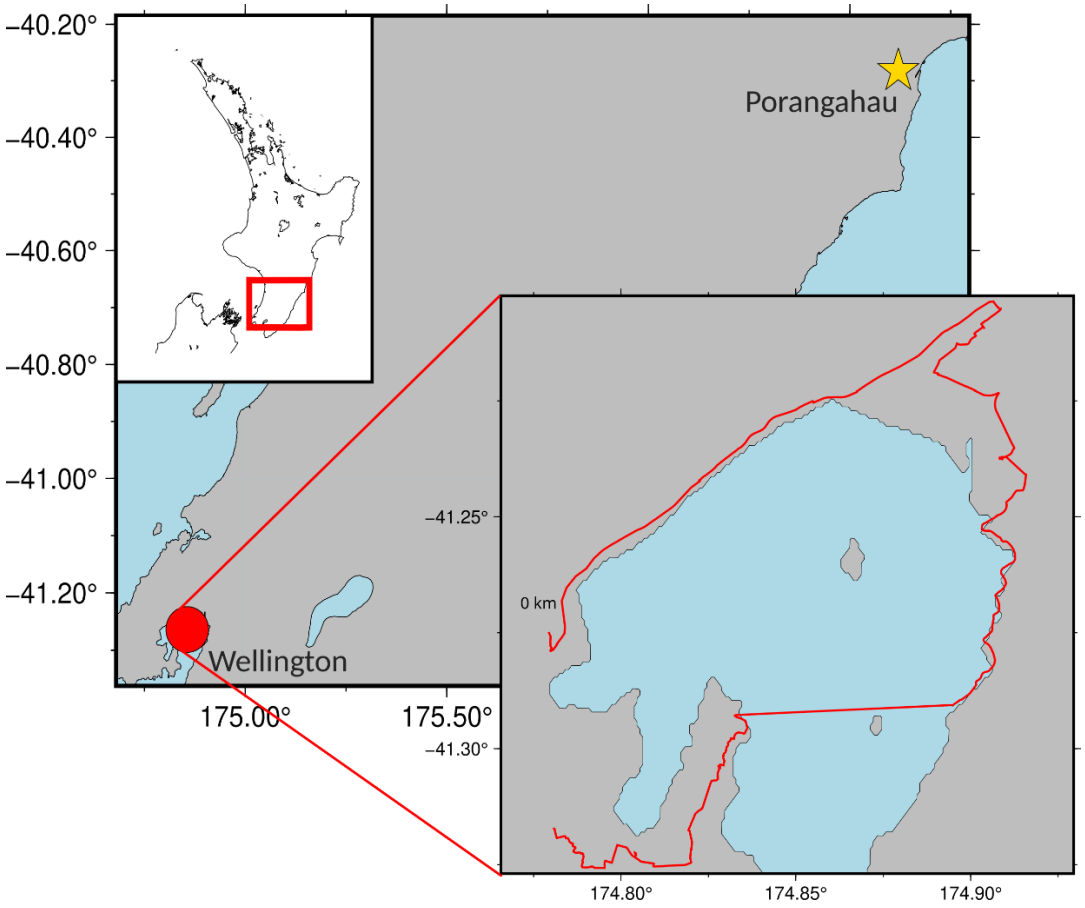

Figure 8: Location of Wellington Fibre and M5.9 Porangahau earthquake analysed.

FK-filtering involves the computation of a two-dimensional Fourier transform from time and space domains to frequency and wavenumber. Within the FK-domain, a filter-window or mute is designed to remove noisy data. Such filter-windows are usually designed to minimise filter artefacts, although in our simple trials we used simple filter-windows with hard cuts at the edges and so expect filter artefacts in our filtered data. After muting, the data are transposed using a 2D inverse Fourier transform to time and space domain. We designed our filter windows to remove noise associated with vehicle traffic (Figure 9), which appears as coherent linear arrivals along the DAS array travelling much slower than earthquake-related seismic wave arrivals. Due to their difference in moveout or "slowness", these arrivals a readily separated in the FK domain, meaning that such noise can be suppressed (Figure 10).

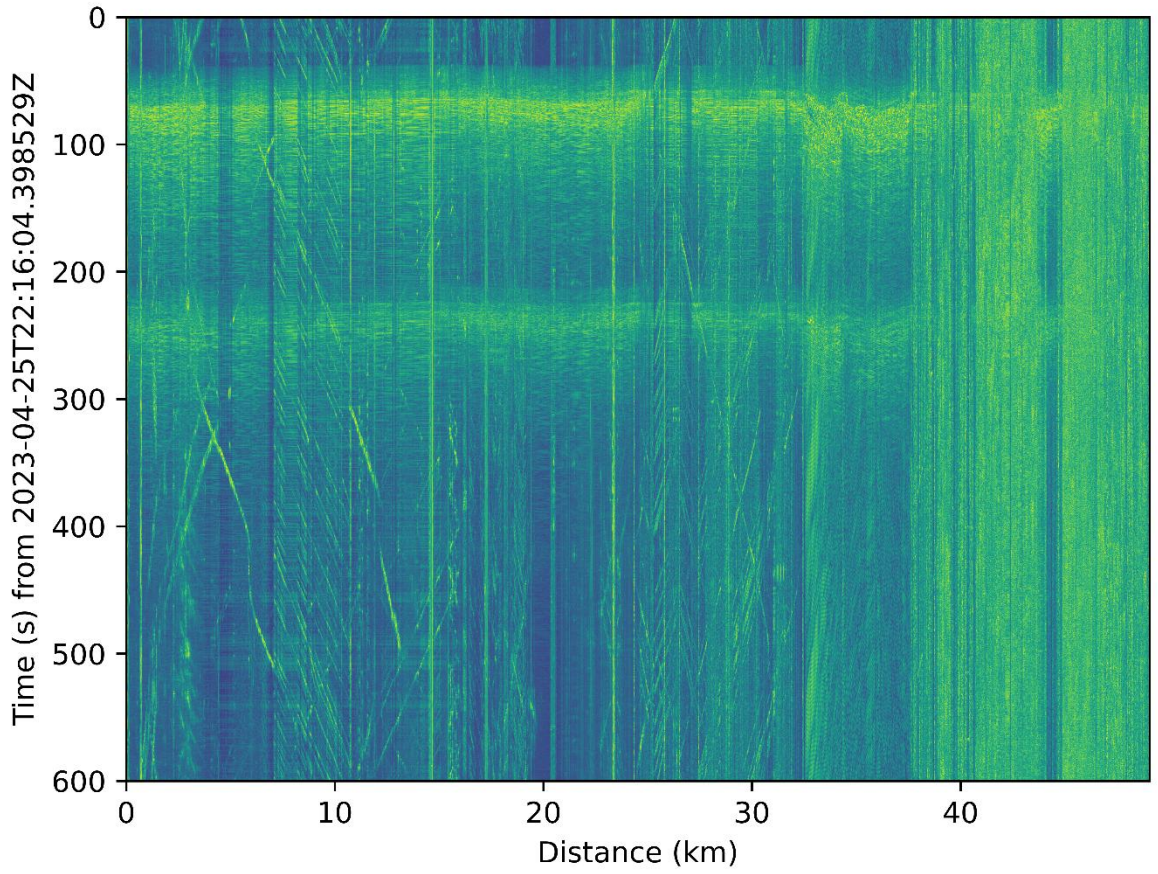

Figure 9: Unfiltered DAS data from the Wellington fibre for the M5.9 Porangahau earthquake (P arrival ~50s). Note aftershock at ~220s and strong diagonal linear traffic noise. Bright colours show higher amplitude, amplitudes are not converted to seismic ground motion.

We applied matched-filter methods to both conventional data and DAS data (both FK-filtered and unfiltered). We compare all earthquake catalogues to the GeoNet catalogue for the 4-day analysis time period. To compute matched-filter detections we used the EQcorrscan Python package (Chamberlain et al., 2018). We note that this package was designed to work with conventional seismic data from tens of stations: a major component of work in this project has been to increase the memory efficiency of EQcorrscan to enable the processing of DAS data.

Matched-filter methods require template waveforms which are then used to compare to continuous data. Detections are made when the cross-correlations, summed across all channels, between a template event and the continuous waveforms, exceeds a threshold. This method is well suited to earthquake sequences where events within a sequence come from a similar location and are likely to have similar waveforms. However, matched-filters are poorly suited to the general earthquake detection case where no prior knowledge of the earthquake waveforms is available.

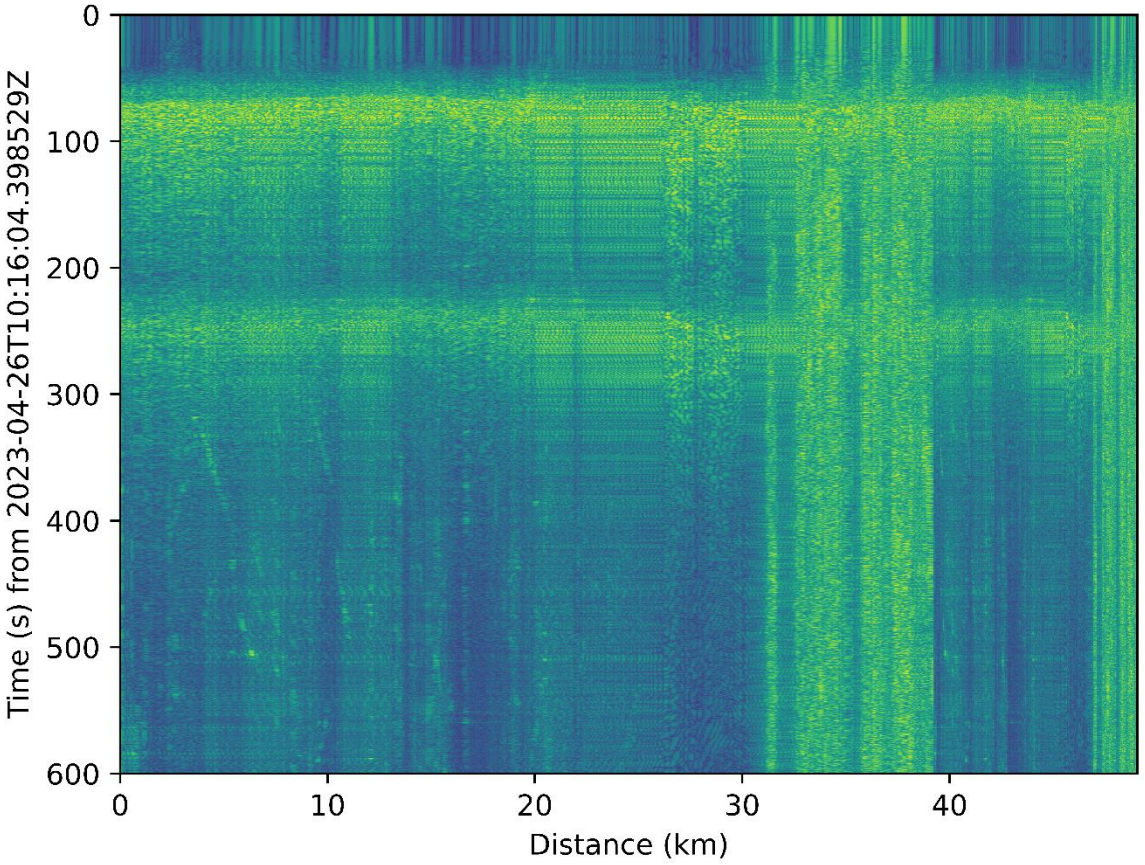

Figure 10: FK-filtered DAS data covering the same period as in Figure 9. Note the reduction in diagonal traffic noise, but the introduction of "ringing" artefacts introduced by the simple filter window applied.

Template construction for matched-filter analysis requires the accurate picking of earthquake arrival times which are then used to extract relevant waveforms from the continuous data. We trialled three methods for picking of earthquake phase arrivals using DAS data. These methods were: 1) manual phase picking; 2) correlation guided picking from original manual picks; and 3) automated picking using routines designed for conventional seismic data. Manual phase picking of data is a slow process, but we adapted existing pick-review code to speed up the process. Nevertheless, it took on the order of hours to manually pick a single earthquake, which motivated us to trial other automated routines.

The second method we trialled uses one manual phase pick on a single DAS channel to guide a cross-correlation picker. In this method data from one channel is compared to the next channel to find the optimal shift to align the data. This method relies on the similarity of waveforms on adjacent segments of DAS fibre. We trialled correlating all DAS channels with the single picked channel, but found that this resulted in low correlation values, particularly on segments of cable in different orientations to the orientation of the original picked channel. We also trialled correlation between adjacent channels, with pick shifts propagated along the fibre. This worked well for high signal-to-noise traces, but was

prone to mis-picking on low signal-to-noise traces, which led to subsequent pick-drift and increasing inaccuracy for channels further along the fibre.

The final methods we trialled were the use of existing picking methods designed for conventional data. We trialled both an energy-based detector known as the sta/lta method (short-term average/long-term average amplitude), which is a well-used method, and a more modern machine-learning derived method known as EQTransformer (Mousavi et al., 2020). EQTransformer has shown good results on conventional data throughout New Zealand, but generally requires three-component data to operate most effectively. We found that the sta/lta detector was effective, but prone to false detections on noisy data, particularly associated with traffic noise. We found that while EQTransformer performed moderately well, making picks on the majority of channels picked manually, the picks made using EQTransformer were not accurate enough to be used to define matched-filter templates.

The knowledge gained in testing earthquake phase pickers has been directly used to inform two subsequence MSc projects funded through the NHC Toka Tū Ake University Research Programme in Earthquake Seismology and Tectonic Geodesy led by Townend and Chamberlain. This work has analysed data collected on a section of fibre near Haast, compared to earthquake datasets collected using conventional seismic data. This region provided a more suitable extended test case for these earthquake detection methods than the city-based fibres targeted in this study mostly due to the greater availability of high-quality earthquake catalogues from other analyses. We note that since starting work on this, a DAS-specific machine-leaning picking code has been released, known as PhaseNetDAS (Zhu et al., 2023), which we have trialled using the Haast fibre. This code has given good results and we expect this would be a useful tool for monitoring unrest using DAS data, however we have not conducted a comparison for the detection limits compared to matched-filter analysis.

To test the efficacy of matched-filter detection applied to DAS data we used a single template event constructed using manually picked phase arrivals from the April 2023 M5.9 Porangahua earthquake. We used the same template event picked on conventional seismometers to compare to the detections made by DAS, as well as comparison to the GeoNet catalogue. We note that we were limited to a single event mostly due to the time constraints posed by manual picking of the DAS data. Following the testing and development of an automated DAS event detection pipeline undertaken by MSc student Isabella Sulvaran, future matched-filter analysis could make use of picks using this pipeline to define templates.

The DAS template was constructed using 3,054 channels of data from the Wellington fibre, with template waveforms starting 0.5 s before the manually picked P phase arrival. Template waveforms were cut to 20 s to capture the P, S and coda waves. Data were filtered between 1—9 Hz prior to trimming to enhance the signal-to-noise ratio of the data, and resampled to 20 Hz to increase computational efficiency. We generated similar template waveforms for conventional seismic data, but used P picks available in the GeoNet catalogue and used all stations picked by GeoNet.

We correlated these templates with 4 days of data starting at the time of the mainshock. To fit the DAS dataset within memory we split the dataset into 30-minute chunks overlapping by roughly 1 minute. For the conventional seismic data we used day-long chunks overlapped by a similar amount. We found that for the DAS data, using the full cable length resulted in spurious detections associated with noise from the section of cable poorly coupled to the ground. We therefore only correlated with the first 2,400 channels. We correlated with both FK-filtered and non-FK-filtered DAS data. In all cases the data were otherwise processed in the same way as the templates (frequency filtered and resampled).

Results and Discussion

Matched-filter analysis of conventional seismic data as described above yielded 24 unique detections for the four days of analysis surrounding the M5.9 Porangahau earthquake (Figure 11). 19 of these detections have very low signal to noise ratios in Wellington. Three of these detections are not in the GeoNet catalogue, but appear to be good detections. Further analysis would be required to determine a final catalogue (following workflows such as that employed by Warren-Smith et al. (2017)).

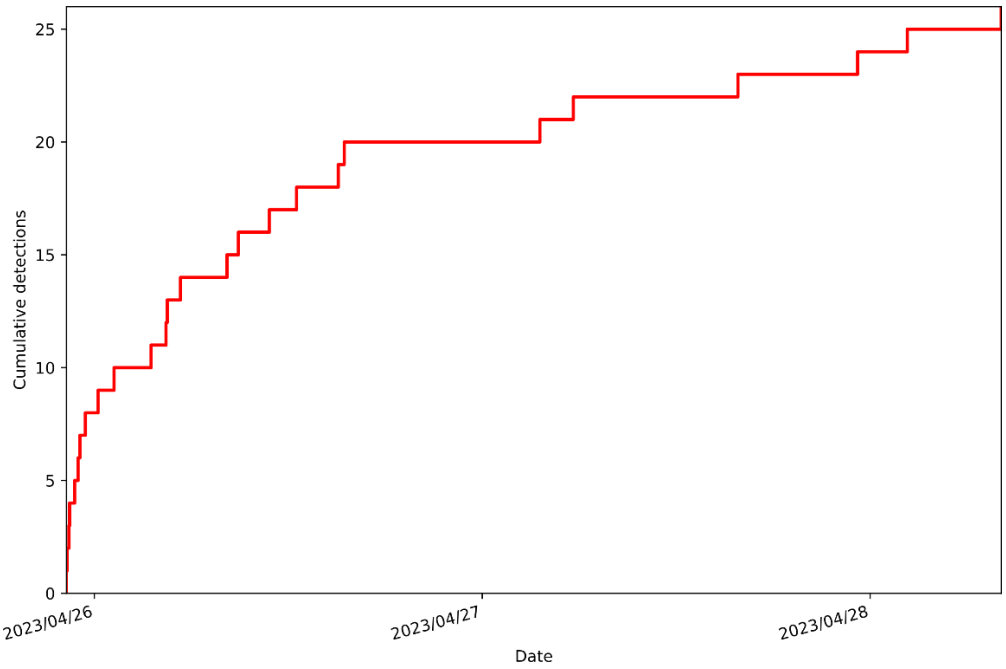

Figure 11: Matched-filter detection times using conventional seismic data following the M 5.9 Porangahau earthquake.

Matched-filter analysis applied to non-FK-filtered data from the Wellington fibre resulted in 36 detections following the removal of detections within 2s of each other, however we note that there likely remain duplicate detections within this dataset as shown by the spikes in Figure 12. Several of these detections are correlated in time with GeoNet catalogued earthquakes, including the M3.9 aftershock shown in Figure 13. We note that in general seismic phases for aftershocks of this sequence are most visible on channels between roughly 4—16km fibre distance, which corresponds to the section of the cable running along SH2. It is likely that this relates to the single-direction sensitivity of the fibre, with this section of the fibre being best oriented for P polarised particle motion. It is

possible that the later phase visible between 19—25 km fibre distance is a seismic phase arrival with a different polarisation which that section of the fibre is more sensitive to.

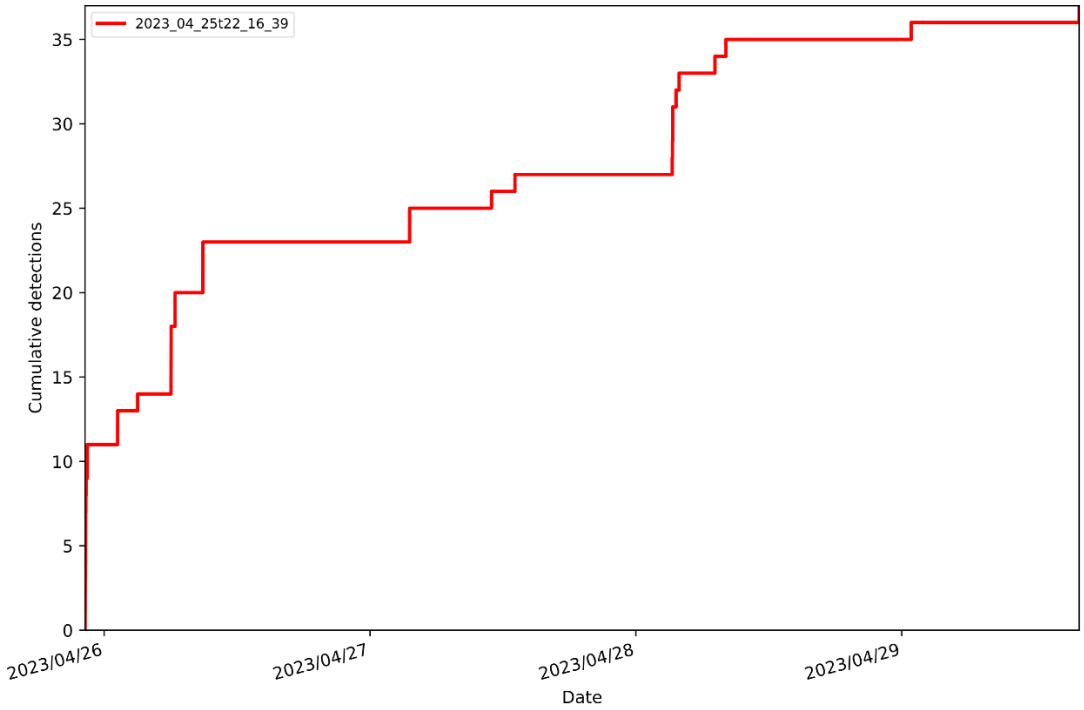

Figure 12: Matched-filter detection times using non-FK filtered DAS data. Detections within 2 s of other detections have been removed, however some duplicate detections likely remain as shown by steps of multiple detections close in time.

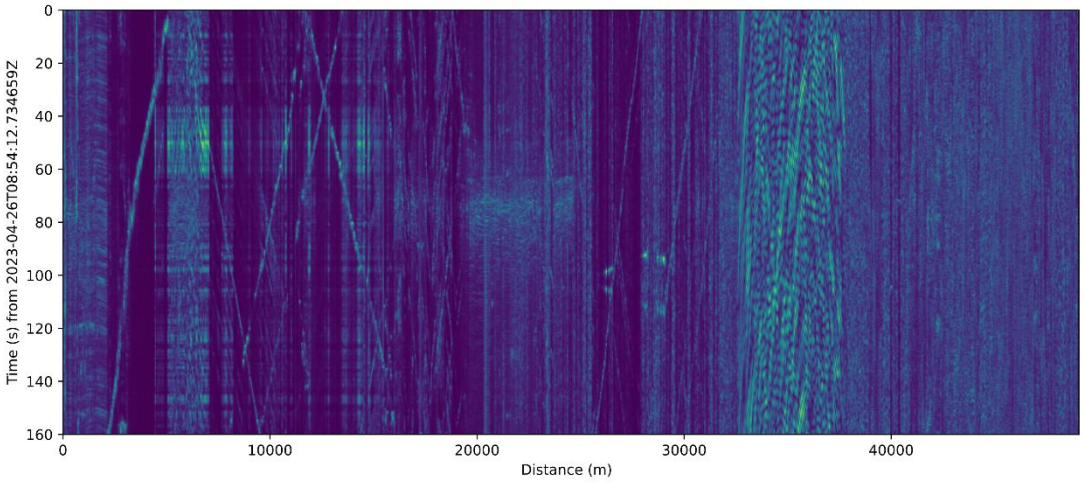

Figure 13: Detection of M3.9 Porangahau aftershock (GeoNet ID: 2023p311814) on the Wellington fibre. P phase arrival at ~40s most visible between 5-15 km fibre distance. Possible later arriving phase is also visible around 60s between distances 19-25km.

FK-filtering of the DAS data visually reduces the impact of linear traffic noise (Figure 10) resulting in differing detections (Figure 14). Using the same workflow as applied to the

non-FK-filtered data, but using the FK-filtered data we obtain similar numbers of detections, but we note that there appear to be many more duplicate detections early in the sequence, with few detections in the middle of the time period analysed compared to the non-FK filtered data.

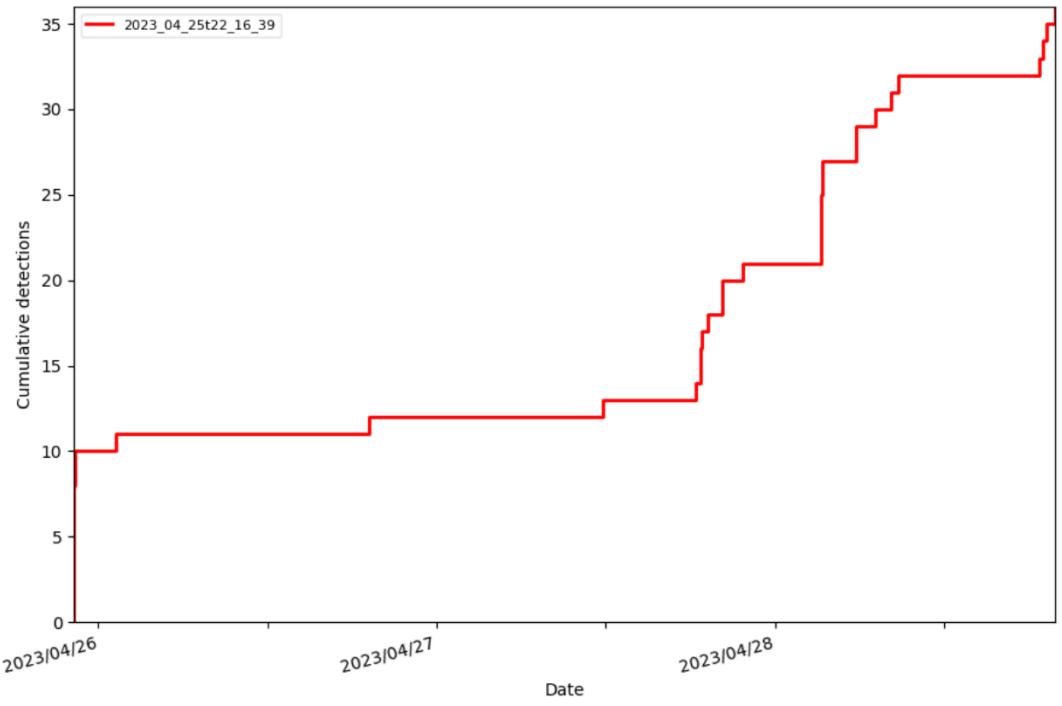

Figure 14: Matched-filter detections using the FK-filtered fibre data. Detections within 2s of other detections have been removed, but some duplicate detections likely remain as shown by the large steps in the detection time-series.

Of the detections made using both the FK-filtered and non-FK-filtered DAS data, there is a low rate of false detections (determined by visual inspection of waveforms), but high rates of duplicate detections. There is also significant overlap between detections made using DAS data and the GeoNet catalogue. We also note that at least one detection exists for an earthquake not located near the template event, suggesting poor sensitivity to earthquake location. It is likely that many of the duplicate detections in the FK-filtered matched-filter analysis result from filter artefacts due to the simplistic approach for filter-

window design used in this analysis. More refinement of this filter window may result in fewer duplicate detections.

Conclusions and Recommendations

Matched-filter analysis is a promising earthquake detection technique for DAS data in urban settings, however we found that matched-filters applied to DAS data alone suffered from duplicate detections. We also found that earthquakes not located close to our template event were detected suggesting weak constraints on earthquake location. Both the duplicate detections and detection of events not linked to the template events is likely due to the relatively small moveouts across the fibre. We suggest that this could be ameliorated by incorporating data from other seismic sensors in different locations unto the matched-filter process. Such incorporation would require weighting of the correlations to ensure that the DAS data did not dominate the correlation sum.

We also found that FK-filtering was effective at removing linear traffic noise from DAS data, however our simplistic approach to filter design resulted in strong filter artefacts. Nevertheless, matched-filter detection applied to FK-filtered data yielded additional detections that were not possible using non FK-filtered data, suggesting that there is value in suppressing this traffic noise. We recommend a more careful approach to filter design, or the use of more advanced methods such as the machine learning methods pioneered by Konietzny et al. (2024).

Publications, communications and engagement

Chamberlain, C.J., McNab, A., Lindsey, N., Van Wijk, K. & Townend, J. (2024). Matched-filter earthquake detection applied to city-scale DAS fibre-optic systems in Aotearoa New Zealand: what more can we detect? *Seismological Society of America Annual Meeting 2024*. Poster presentation

O'Hagan, S. (2025). Constraining earthquake rates at the Auckland Volcanic Field 2011-2022. *VUW MSc thesis*. Supervised by Chamberlain, C.J.

Data Availability

The catalogues (earthquakes, blasts and unclassified) generated in this research for the Auckland Volcanic Field is available online (https://zenodo.org/records/15825886, last accessed 16/09/2025). These catalogues were constructed using open-access GeoNet data. The DAS data are not available due to commercial sensitivity.

References

Chamberlain, C., & Townend, J. (2018). Detecting real earthquakes using artificial earthquakes: On the use of synthetic waveforms in matched-filter earthquake detection. *Geophysical Research Letters*, *45*(21), 11,641-611,649.

Chamberlain, C. J., Hopp, C. J., Boese, C. M., Warren-Smith, E., Chambers, D., Chu, S. X., Michailos, K., & Townend, J. (2018). EQcorrscan: Repeating and near-repeating earthquake detection and analysis in python. *Seismological Research Letters*, *89*(1), 173-181. https://doi.org/10.1785/0220170151 ,

Christophersen, A., Bourguignon, S., Rhoades, D. A., Allen, T. I., Salichon, J., Ristau, J., Rollins, C., & Gerstenberger, M. C. (2022). *Consistent magnitudes over time for the revision of the New Zealand National Seismic Hazard Model*. GNS Science = Te P \=u Ao. https://doi.org/10.21420/A2SN-XM76

Eberhart-Phillips, D., Reyners, M., Bannister, S., Chadwick, M., & Ellis, S. (2010). Establishing a Versatile 3-D Seismic Velocity Model for New Zealand. *Seismological Research Letters*, *81*. https://doi.org/10.1785/gssrl.81.6.992

Ensing, J. X., van Wijk, K., & Spörli, K. B. (2017). Probing the subsurface of the Auckland Volcanic Field with ambient seismic noise. *New Zealand Journal of Geology and Geophysics*, *60*(4), 341-352. https://doi.org/10.1080/00288306.2017.1337643 ,

Ensing, J. X., van Wijk, K., & Spörli, K. B. (2022). A 3D crustal shear speed model of the Auckland volcanic field, New Zealand, from multi-component ambient noise tomography. *Tectonophysics*, *845*. https://doi.org/10.1016/j.tecto.2022.229627

Hopkins, J. L., Smid, E. R., Eccles, J. D., Hayes, J. L., Hayward, B. W., McGee, L. E., van Wijk, K., Wilson, T. M., Cronin, S. J., Leonard, G. S., Lindsay, J. M., Németh, K., & Smith, I. E. M. (2021). Auckland Volcanic Field magmatism, volcanism, and hazard: a review. *New Zealand Journal of Geology and Geophysics*, *64*(2-3), 213-234. https://doi.org/10.1080/00288306.2020.1736102 ,

Kennett, B. L. N., & Engdahl, E. R. (1991). Traveltimes for global earthquake location and phase identification. *Geophysical Journal International*, *105*(2), 429-465. https://doi.org/https://doi.org/10.1111/j.1365-246X.1991.tb06724.x

Konietzny, S., Lai, V. H., Miller, M. S., Townend, J., & Harmeling, S. (2024). Unsupervised coherent noise removal from seismological distributed acoustic sensing data. *Journal of Geophysical Research: Machine Learning and Computation*, *1*(4), e2024JH000356.

Langridge, R. M., Ries, W. F., Litchfield, N. J., Villamor, P., Dissen, R. J. V., Barrell, D. J. A., Rattenbury, M. S., Heron, D. W., Haubrock, S., Townsend, D. B., Lee, J. M., Berryman, K. R., Nicol, A., Cox, S. C., & Stirling, M. W. (2016). The New Zealand Active Faults Database. *New Zealand Journal of Geology and Geophysics*, *59*(1), 86--96. https://doi.org/10.1080/00288306.2015.1112818 ,

Li, J., Zhu, W., Biondi, E., & Zhan, Z. (2023). Earthquake focal mechanisms with distributed acoustic sensing. *Nature Communications*, *14*(1), 4181.

Li, Z., & Zhan, Z. (2018). Pushing the limit of earthquake detection with distributed acoustic sensing and template matching: A case study at the Brady geothermal field. *Geophysical Journal International*, *215*(3), 1583-1593.

Lindsey, N. J., & Martin, E. R. (2021). Fiber-Optic Seismology. *Annual Review of Earth and Planetary Sciences*, *49*, 309-336.

Lindsey, N. J., Martin, E. R., Dreger, D. S., Freifeld, B., Cole, S., James, S. R., Biondi, B. L., & Ajo-Franklin, J. B. (2017). Fiber-optic network observations of earthquake wavefields. *Geophysical Research Letters*, *44*(23), 11,792-711,799.

Lindsey, N. J., Rademacher, H., & Ajo-Franklin, J. B. (2020). On the broadband instrument response of fiber-optic DAS arrays. *Journal of Geophysical Research: Solid Earth*, *125*(2), e2019JB018145.

Lomax, A., Virieux, J., Volant, P., & Berge-Thierry, C. (2000). Probabilistic earthquake location in 3D and layered models. In *Advances in seismic event location* (pp. 101-134). Springer.

Mousavi, S. M., Ellsworth, W. L., Zhu, W., Chuang, L. Y., & Beroza, G. C. (2020). Earthquake transformer—an attentive deep-learning model for simultaneous earthquake detection and phase picking. *Nature Communications*, *11*(1). https://doi.org/10.1038/s41467-020-17591-w

Mousavi, S. M., Sheng, Y., Weiqiang, Z., & Beroza, G. (2019). STanford EArthquake Dataset (STEAD): A Global Data Set of Seismic Signals for AI. *IEEE Access*, *PP*, 1-1. https://doi.org/10.1109/ACCESS.2019.2947848

Münchmeyer, J. (2024). PyOcto: A high-throughput seismic phase associator. *Seismica*, *3*(1). https://doi.org/10.26443/seismica.v3i1.1130

Nayak, A., Ajo-Franklin, J., & Team, I. V. D. F. (2021). Distributed Acoustic Sensing Using Dark Fiber for Array Detection of Regional Earthquakes. *Seismological Society of America*, *92*(4), 2441-2452.

Pita-Sllim, O., Chamberlain, C. J., Townend, J., & Warren-Smith, E. (2023). Parametric testing of EQTransformer's performance against a high-quality, manually picked catalog for reliable and accurate seismic phase picking. *The Seismic Record*, *3*(4), 332-341.

Sherburn, S., Scott, B. J., Olsen, J., & Miller, C. (2007). Monitoring seismic precursors to an eruption from the Auckland Volcanic Field, New Zealand. *New Zealand Journal of Geology and Geophysics*, *50*(1), 1-11.

van den Ende, M. P., & Ampuero, J.-P. (2021). Evaluating seismic beamforming capabilities of distributed acoustic sensing arrays. *Solid Earth*, *12*(4), 915-934.

Van Wijk, K., J. Chamberlain, C., Lecocq, T., & Van Noten, K. (2021). Seismic monitoring of the Auckland Volcanic Field during New Zealand's COVID-19 lockdown. *Solid Earth*, *12*(2), 363-373. https://doi.org/10.5194/se-12-363-2021 ,

Warren-Smith, E., Chamberlain, C. J., Lamb, S., & Townend, J. (2017). High-precision analysis of an aftershock sequence using matched-filter detection: The 4 May 2015 ML 6 Wanaka Earthquake, Southern Alps, New Zealand. *Seismological Research Letters*, *88*(4), 1065-1077. https://doi.org/10.1785/0220170016 ,

Woollam, J., Münchmeyer, J., Tilmann, F., Rietbrock, A., Lange, D., Bornstein, T., Diehl, T., Giunchi, C., Haslinger, F., & Jozinović, D. (2022). SeisBench—A toolbox for machine learning in seismology. *Seismological Society of America*, *93*(3), 1695-1709.

Zhu, W., Biondi, E., Li, J., Yin, J., Ross, Z. E., & Zhan, Z. (2023). Seismic arrival-time picking on distributed acoustic sensing data using semi-supervised learning. *Nature Communications*, *14*(1), 8192.

Zhu, W., McBrearty, I. W., Mousavi, S. M., Ellsworth, W. L., & Beroza, G. C. (2022). Earthquake Phase Association Using a Bayesian Gaussian Mixture Model. *Journal of Geophysical Research: Solid Earth*, *127*(5). https://doi.org/https://doi.org/10.1029/2021JB023249